REPORT DOCUMENTATION PAGE

Form Approved
OMB No. 0704-0188

PLEASE DO NOT RETURN YOUR FORM TO THE ABOVE ADDRESS.

1. REPORT DATE *(DD-MM-YYYY)*	2. REPORT TYPE	3. DATES COVERED *(From - To)*
01012008	Journal Article	

4. TITLE AND SUBTITLE

3D underwater imaging using vector acoustic sensors

5a. CONTRACT NUMBER

5b. GRANT NUMBER

5c. PROGRAM ELEMENT NUMBER

61153N

6. AUTHOR(S)

Dennis Lindwall

5d. PROJECT NUMBER

5e. TASK NUMBER

5f. WORK UNIT NUMBER

7. PERFORMING ORGANIZATION NAME(S) AND ADDRESS(ES)

Naval Research Laboratory
Marine Geoacoustics Division
Stennis Space Center, MS 39529

8. PERFORMING ORGANIZATION REPORT NUMBER

NRL/JA/7430-06-2

9. SPONSORING/MONITORING AGENCY NAME(S) AND ADDRESS(ES)

Office of Naval Research
800 North Quincy Street
Arlington VA 22217-5000

10. SPONSOR/MONITOR'S ACRONYM(S)

ONR

11. SPONSOR/MONITOR'S REPORT NUMBER(S)

12. DISTRIBUTION/AVAILABILITY STATEMENT

Approved for public release; distribution is unlimited

13. SUPPLEMENTARY NOTES

GEOPHYSICS, VOL 73, NO. 1 (JANUARY-FEBRUARY 2008); P-Q1-17, 11FIGS. 10.1190/1.2813347

14. ABSTRACT

Marine surveys that use vector acoustic sensors may allow for 3D imaging of underwater environments with a much smaller amount of data than current 3D hydrophone surveys. Newly developed sensors make vector-acoustic-based surveys practical. This concept is demonstrated with data from a three-axis accelerometer and a collocated hydrophone in an acoustic water tank using a short-pulse source and passive scattering targets. One algorithm rectifies the vector data with scalar pressure data and another maps the vector data into a 3D volume, showing several slices of the volume images.

15. SUBJECT TERMS

16. SECURITY CLASSIFICATION OF:			17. LIMITATION OF ABSTRACT	18. NUMBER OF PAGES	19a. NAME OF RESPONSIBLE PERSON
a. REPORT	b. ABSTRACT	c. THIS PAGE			Dennis Lindwall
Unclassified	Unclassified	Unclassified	UU	7	19b. TELEPHONE NUMBER *(Include area code)* 228-688-5306

GEOPHYSICS, VOL. 73, NO. 1 (JANUARY-FEBRUARY 2008); P. Q1–Q7, 11 FIGS.
10.1190/1.2813347

3D underwater imaging using vector acoustic sensors

Dennis Lindwall[1]

ABSTRACT

Marine surveys that use vector acoustic sensors may allow for 3D imaging of underwater environments with a much smaller amount of data than current 3D hydrophone surveys. Newly developed sensors make vector-acoustic-based surveys practical. This concept is demonstrated with data from a three-axis accelerometer and a collocated hydrophone in an acoustic water tank using a short-pulse source and passive scattering targets. One algorithm rectifies the vector data with scalar pressure data and another maps the vector data into a 3D volume, showing several slices of the volume images. The imaging algorithm maps the scattered energy using the direction and traveltime independently for each source-receiver pair rather than using the phase coherence methods common in exploration seismology. Imaging a more complex and realistic marine environment requires vector wavefield decomposition techniques and other theoretical developments but may allow for 3D vector-acoustic seismic surveys using logistics similar to 2D surveys that use conventional hydrophones.

INTRODUCTION

Vector acoustic sensors measure either the particle motion or the pressure gradient from passing acoustic waves and produce three- or four-component (3-C or 4-C) data (Fahy, 1977, 1989; Berliner and Lindberg, 1996). Vector acoustic data include directional information that may allow for 3D acoustic imaging with significantly less data than required with hydrophone data. Using a vector sensor with a controlled-pulse source, one can determine both distance and direction for the sound source as well as scattering and reflection points.

Geophones, which usually measure displacement, have been used to measure local particle motion in the solid earth since the start of observational seismology. One significant technical difficulty with geophones is the coupling between the solid earth and the sensors as well as the device resonances (D'Spain et al., 1991). Using geophones in water poses different coupling problems, but new developments in miniature accelerometers that allow for the construction of small, rigid, neutrally buoyant sensors allow for much better coupling between the sensors and the local particle motion (Shipps and Deng, 2003). Towing an accelerometer-based sensor through the water, such as in a streamer, would require a more practical suspension solution than the one used in our experiment while minimizing the flow noise. The three separate accelerometer components, as well as an accompanying hydrophone, also must be matched in their phase and frequency response.

Data from vector acoustic sensors used in geoacoustic surveys of the seafloor provide additional directional information not present in scalar pressure data from traditional hydrophones (Lindwall, 2006). Hydrophone arrays for use in seismic profiling and seafloor imaging surveys such as side-scan sonar need to be about 20 wavelengths long to provide a directional resolution of 1° or 2° (Kinsler et al., 1982). Unambiguous determination of direction requires three orthogonal arrays of scalar sensor arrays, a configuration that is cumbersome and impractical. A combined vector sensor and controlled source give both distance and direction for the sound source as well as scattering and reflection points.

In principle, a single sound pulse recorded at a single vector acoustic sensor can provide a 3D acoustic picture of the local environment. In practice, numerous ambiguities are caused by overlapping arrivals from different scattering points. These ambiguities can be resolved with a single line of source or sensor locations in most cases. Data from a linear hydrophone array can, at best, give only a 2D image of the environment from the same survey configuration. For specular reflections, adequate illumination of reflective surfaces may require multiple source and receiver locations.

In this paper, I show how a vector acoustic sensor may be used for underwater applications. I also show that vector acoustic data can be acquired with existing sensors and that images of scatterers in a 3D volume can be made with a rather small amount of data. This is verified by an experiment using an accelerometer-based vector acoustic sensor in a water tank with a short-pulse source and passive scattering targets. I present an algorithm for rectifying the vector data with scalar pressure data and an algorithm for mapping the vector data

Manuscript received by the Editor 12 December 2006; revised manuscript received 7 September 2007; published online 12 December 2007.
[1]Naval Research Laboratory, Marine Geosciences Division, Stennis Space Center, Mississippi, U.S.A. E-mail: lindwall@nrlssc.navy.mil.

into a 3D volume. I then show several slices of the resulting volume images.

THE EXPERIMENT

The data from the experiment were acquired with a TV-001 miniature vector sensor designed for use in water by Roger Richards and others of the NAVSEA division of the Naval Underwater Warfare Center in conjunction with Wilcoxon Research Inc. (Shipps and Deng, 2003). The sensor contains a three-axis accelerometer and a hydrophone, has a sensitivity of 1.0 V/g and a frequency response of about 3 Hz to 9 kHz, has the shape of a cylinder with two hemispherical end caps, and is 71 mm long and 41 mm in diameter with a mass of 54 g. This sensor is nearly neutrally buoyant in water so as to have the best motion coupling with the water.

Figure 1 shows the tank configuration. The vector sensor was suspended near the center using a tether arrangement similar to that shown in Shipps and Deng (2003, their Figure 2). This tether arrangement had a resonant frequency of approximately 1 Hz, well outside of our data band, and allowed the sensor to couple well with the local particle motion. The electrical data cables were left slightly slack to minimize their interference with the motion of the sensor. The sound source was a single transducer driven using a synthesized Ricker wavelet with a median frequency of 7 kHz, moved along several straight lines while the sensor remained stationary.

After shooting several reference lines, two air-filled floats were placed in the water as highly reflective scattering targets. All of the data presented in this article have the target floats in the same horizontal plane as the source and receiver, whereas the processing and imaging retained the 3D approach. This is to present the concepts of vector acoustic data in the simplest form.

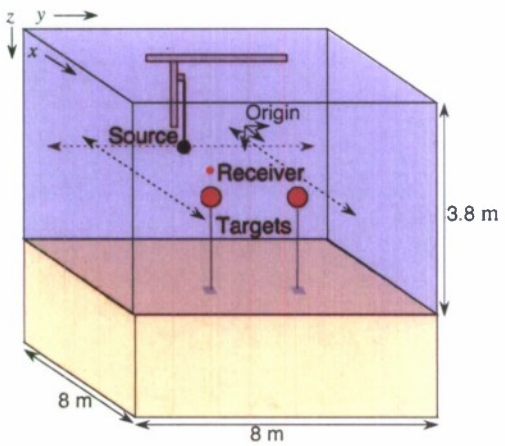

Figure 1. The experimental setup was in a water tank with a sand bottom designed specifically for acoustic experiments. The receiver consists of a three-axis accelerometer and a hydrophone. The receiver was suspended by several thin elastic strands (not shown) and was stationary throughout the experiment. The acoustic transponder source was attached to a robot that could move in three dimensions and was computer controlled for automated data collection. The targets were air-filled floats and were placed in several positions. The data in this article were taken with both targets in the same horizontal plane as the source and receiver. The receiver, targets, and source were 2 m below the water surface; the three source lines, shown as dashed lines, were offset 1 m from the receiver, the vector sensor receiver was at (1.527, 1.19, 0), and the targets were at (2.417, 1.85, 0) and (2.497, 0.64, 0) in (x,y,z) coordinates in meters.

Figure 2 shows common-receiver-point gathers of the accelerometer and hydrophone data. The direct arrival from the source is the most prominent signal and is hyperbolic with a phase shift apparent in the apex of the y-component data. The main pulse of the signal has a delay of 1.5 ms from the time break. Unfortunately, this 1.5-ms delay is filled with noise caused by flaws in the synthesis of the Ricker wavelet. This noise degrades the images shown later. The sandy bottom of the tank and the water-surface reflections are visible as hyperbolic reflections, with their apexes at the same offset as the direct arrival and times of 3.9 and 4.5 ms. The scattered waves from target floats in the tank show up as similar hyperbolic reflections with apexes that are offset to the sides and beginning times of about 3.5 ms.

DIRECTIONALITY, INTENSITY, AND FIDELITY

Acoustic intensity **I** is the energy flux caused by passing sound waves, quantified by

$$\mathbf{I} = p\mathbf{v}, \tag{1}$$

where p is the pressure and v is the particle velocity (Pierce, 1981, equation 1-11.3). Ideally, we would measure the acoustic intensity at

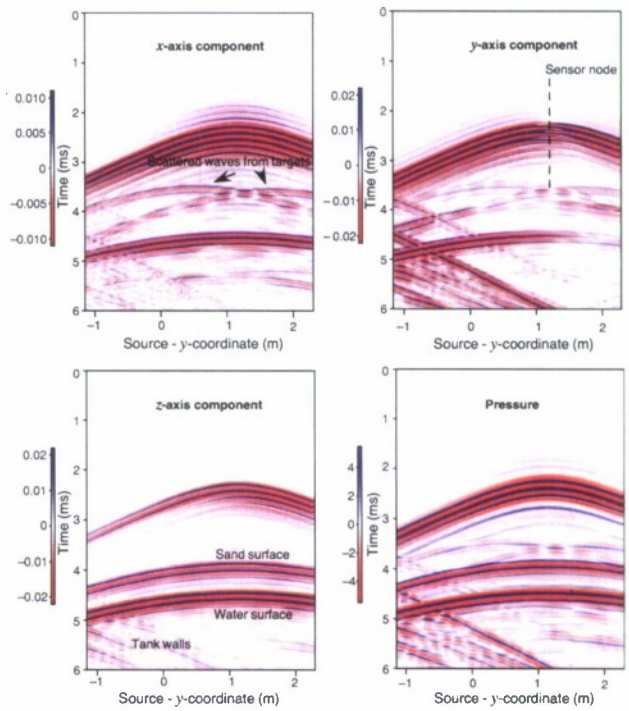

Figure 2. Time-series offset plots of the accelerometer components and the hydrophone for a data set acquired while moving the source along the y-axis from $(0.52, -1.11, 0)$ to $(0.52, 2.29, 0)$ in (x,y,z) coordinates in meters. The direct arrival from the source appears as the prominent hyperbolic signal in all channels with the y-axis node and phase shift at the hyperbola's apex. The main pulse of the signal has a delay of 1.5 ms from the time break. The sandy bottom of the tank and the water-surface reflections also appear as hyperbolic reflections, particularly in the z-axis panel, with their apexes at the same offset as the direct arrival and traveltimes of 3.9 and 4.5 ms. The scattered waves from the target floats appear as hyperbolic reflections with apexes at $y = 0.64$ and 1.85 m and traveltimes of about 3.5 ms. The scattered waves from the targets are about 1% of the amplitude of the direct wave.

every sensor location, but there is no such ideal sensor. Motion sensors, such as the accelerometers used in this study, generally have vector fidelity problems, and hydrophones usually measure the velocities of their faceplates rather than the true pressure.

When imaging, we do not need to calculate the true intensity, yet we need some value that resembles it in terms of direction, phase, and amplitude. For a single-axis pressure gradient sensor, the intensity component is defined as

$$I_n = P_1 P_2 \sin(\phi_1 - \phi_2)/2\rho_0 \omega d, \quad (2)$$

where P_1 and P_2 are the pressures at the transducer pairs, ϕ_1 and ϕ_2 are the signal phases at the transducer pairs, ρ_0 is the mean density, ω is the angular frequency, and d is the transducer spacing (Fahy, 1989, equation 5.7).

For accelerometer sensors, there is no precise definition of intensity. Directionality (the accuracy of the direction estimate) depends on good matching of the phase and amplitudes of each axis of the accelerometers or of each hydrophone element of a pressure gradient sensor. The directionality is degraded by mismatched phases, amplitude sensitivity, environmental noise, and vector infidelity. Directionality also can be lost when two waves from different directions arrive simultaneously.

Figure 3 shows a hodograph of the direct arrivals from the x and y accelerometer components with the source at four different locations. This figure illustrates some of the inaccuracies of the sensor and of the experimental setup. Two of the signals are aligned with the x- and y-axes and two are at 45° angles from the axes. The y-axis accelerometer of this sensor is about twice as sensitive as the x-axis accelerometer, and the data shown are corrected for this. The sensor motion from the source in the y-axis direction (green) was aligned well with the y-axis, but the sensor motion from the source in the x direction (red) deviated substantially from the axis. The x-direction motion deviations may have been caused by an internal defect in the sensor or by some motion restrictions from the electrical cables. In spite of the vector fidelity problems with our sensor, we are able to use these data for this demonstration of the vector acoustic imaging concept.

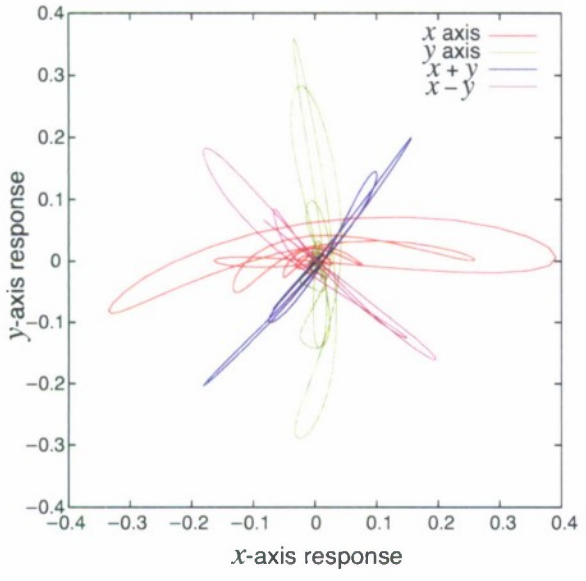

Figure 3. Hodograph of the x and y accelerometer components of direct waves from the source. Two of the signals are from the source aligned with the x- and y-axis, and two are from the source at 45° angles from the axes. The y-axis accelerometer was twice as sensitive as the x-axis accelerometer, and the data have been corrected for this difference.

DETECTION AND LOCATION

The location of a controlled source can be determined with a single vector sensor by measuring the direction and the traveltime of the direct wave. The source position vector **s** is

$$\mathbf{s} = \mathbf{g} + \hat{\mathbf{d}}tc, \quad (3)$$

where **g** is the receiver position, $\hat{\mathbf{d}}$ is the unit vector aligned with the particle motion, t is the traveltime, and c is the sound speed.

Figure 4 shows how a scattering target can be located using known source and receiver locations by measuring the directional response and the traveltime of the scattered waves. Multiple scattering targets can be located with a single vector sensor, provided that the scattered signals are separated in time at the sensor. In the following calculations, the source and receiver positions **s** and **g** are known, and the traveltime t and the vector response of the sensor **d** are measured. The target position vector **e** is calculated by

$$\mathbf{e} = \mathbf{g} + \hat{\mathbf{d}}r, \quad (4)$$

$$r = \frac{b^2 - c^2t^2}{2(b\cos\theta - ct)}, \quad (5)$$

and

$$\theta = \cos^{-1}\left(\frac{\mathbf{d}\cdot(\mathbf{g}-\mathbf{s})}{b|\mathbf{d}|}\right), \quad (6)$$

where r is the range to the target, b is the source to receiver range, **d** is the data vector, $\hat{\mathbf{d}}$ is the data vector of unit length, θ is the angle between the receiver-source and the receiver-target vectors, and $\|$ denotes the norm, or length, of the vector. The large dot denotes the vector dot product.

Figure 5 shows the sensor motions caused by the scattered waves from the targets. This hodograph illustrates the directional information in vector acoustic data. Interference from the direct signals is present, even though these signals were selected for minimum interference. The interference from the direct signal will cause loss of resolution in the target imaging and also may be confused with poor vector fidelity.

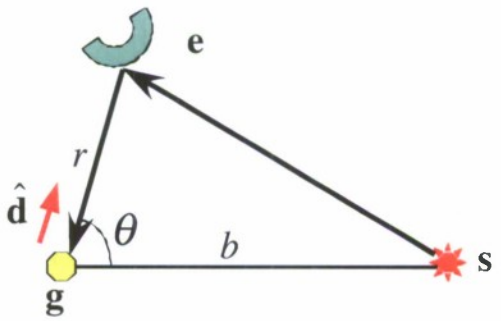

Figure 4. Geometry of the target location. The source and sensor locations **s** and **g** are known, along with their separation b. The recorded data **d** are the vector responses of the sensor.

When multiple scattered signals overlap, such as in the data in Figure 2, then the targets and surfaces cannot be located with a single source and receiver location. Locating each target within a field of scattering targets requires multiple sources or sensors. For most cases, a single line of either source or vector receiver locations is sufficient. A single sensor or receiver will not be able to correctly locate two scattering targets that are positioned symmetrically with respect to the axis of the line. This two-target ambiguity can be resolved in several ways. If either the source or the vector-sensor is held fixed as the other is moved along a line, the fixed device can be off-axis of the line. This reduces the location ambiguity to objects at symmetric positions on a single plane.

All target position ambiguities can be eliminated by moving either the source or the receiver (or both) along a serpentine path. With a serpentine path, there never will be two target positions that always have identical two-way traveltimes. This presumes that the positions of the source and the receiver and the shot times are always known. A vector sensor can, in fact, be used to position itself relative to a sound source if it includes orientation devices, such as a compass and tiltmeters. This eliminates the need for additional positioning systems that are necessary for 3D surveys.

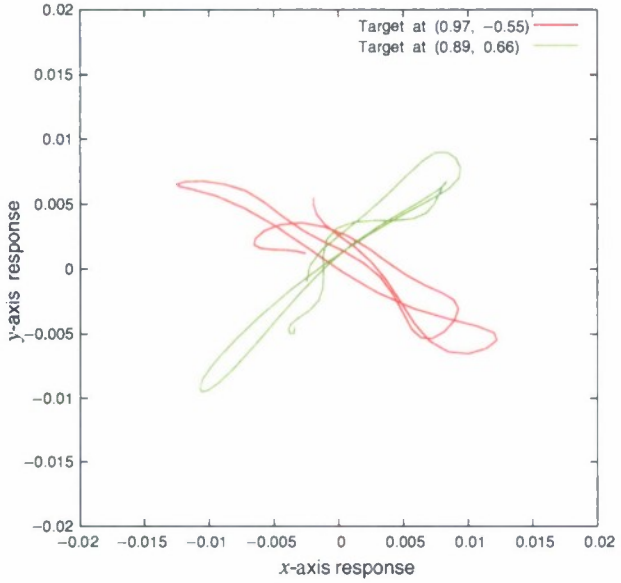

Figure 5. Hodograph of the x and y accelerometer components of the scattered signals from the target floats. The traces were selected at a location where the reflections had the best separation from other signals. The scattered arrivals were time windowed and corrected for the different sensitivity of the x- and y-axis accelerometers. There is some remaining energy from the direct signals that interferes with these scattered signals and shows up as the weaker, sideways wiggling of the signals. The source positions were $(-1.0, -0.75)$ and $(-1.0, 0.9)$, and the sensor was at (0.0, 0.0).

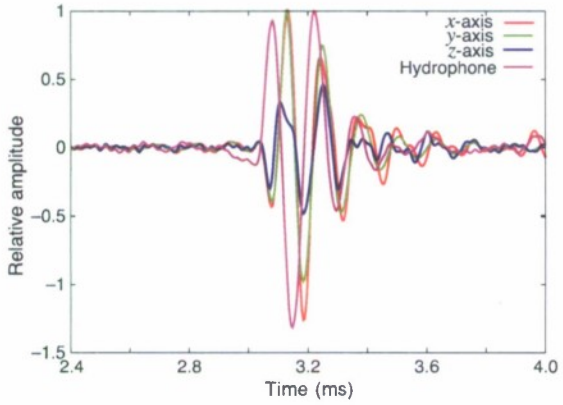

Figure 6. Time series plots of the three accelerometer signals and the hydrophone. The hydrophone response must be corrected to match the response of the accelerometers before using the hydrophone trace to rectify the accelerometer traces.

Rectifying the signal

The direction vector $\hat{\mathbf{d}}$ in equation 3 is proportional to the norm of the time-averaged acoustic intensity $\mathbf{I}$ (D'Spain et al., 1991; Crocker and Arenas, 2003) or to the direction of energy flux vector (Chapman, 2004) and is analogous to the Poynting vector used in electromagnetism. Although the acoustic intensity would be ideal for imaging, the actual sensor measurements are the instantaneous particle accelerations and oscillate between the positive and negative intensity vectors.

The instantaneous accelerations can be easily rectified to give approximate intensity vectors without excessive calculations by using the hydrophone data in conjunction with the accelerometer data. The sensor we used has an integral hydrophone, but its response has a different phase and different frequency than the accelerometers (Figure 6). The hydrophone signal must first be filtered before it can be used to rectify the accelerometer signals, as quantified by

$$a(t) \leftrightarrow A(f) \tag{7}$$

and

$$p(t) \leftrightarrow P(f), \tag{8}$$

where $a(t)$ and $p(t)$ are the time series signals of the time-windowed direct arrivals from the accelerometer and the pressure hydrophone and where $A(f)$ and $P(f)$ are their respective Fourier transforms into the frequency domain.

The original hydrophone spectrum $P_D(f)$ is whitened by dividing it by the direct signal spectrum $P(f)$, then multiplied by the acceler-

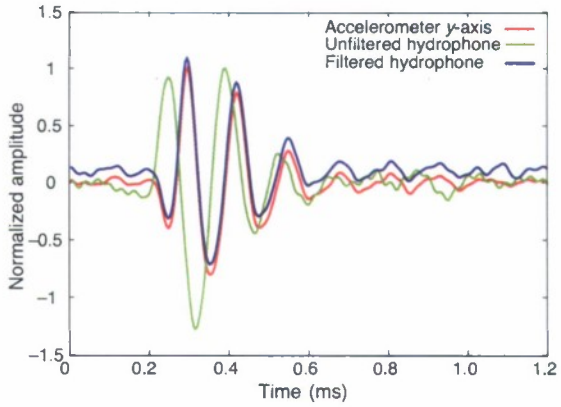

Figure 7. Time series plot of the y-axis accelerometer, the pressure hydrophone, and the spectrum-corrected (filtered) hydrophone signal for the direct arrival only. The filtered hydrophone data are plotted slightly above the accelerometer data. There is an almost exact match between the accelerometer waveform and the filtered pressure waveform.

ometer direct signal spectrum $A(f)$ to give a filtered hydrophone spectrum $P_A(f)$ that can be transformed to the amplitude and phase-matched pressure time series $p_A(t)$ shown in Figure 7. This sequence is represented by

$$P_W(f) = \frac{P_D(f)}{P(f)}, \tag{9}$$

$$P_A(f) = P_W(f) \cdot A(f), \tag{10}$$

and

$$p_A(t) \leftrightarrow P_A(f). \tag{11}$$

The matched pressure time series is used to create the rectifying sign series $\mathrm{sgn}(p_A(t))$ that can change the accelerometer data $a_D(t)$ into rectified accelerometer data $a_R(t)$, as in

$$a_R(t) = \mathrm{sgn}[p_A(t)] \cdot a_D(t). \tag{12}$$

The three rectified accelerometer components can then be combined in the acoustic intensity vector $\mathbf{I}$ (equation 1). If no pressure data are available, the accelerometer data can be partially rectified, if the source wavelet is known, by using the crosscorrelation of the source wavelet $a(t)$ and the accclerometer data $a_D(t)$, given by

$$a_R(t) = \mathrm{sgn}[a_D(t) * a(t)] \cdot a_D(t). \tag{13}$$

As illustrated in the lower plot in Figure 8, equation 13 will not work for phase-shifted reflections, such as from the water surface or air bubbles.

IMAGING

Each source and receiver location $\mathbf{s}$, $\mathbf{g}$ produces a 3-C trace, $\mathbf{d}(\mathbf{s},\mathbf{g},t)$. Equations 3 and 4 map each sample from $\mathbf{d}(\mathbf{s},\mathbf{g},t)$ into a target position vector $\mathbf{e}(\mathbf{s},\mathbf{g},t)$. A volume image can be built by summing the absolute amplitudes $|\mathbf{d}(\mathbf{s},\mathbf{g},t)|$ for all of the recorded traces into their respective volume bins.

Figure 9 shows horizontal slices through three volume images made from three different source lines at the sensor depth, showing the two float targets as well as more distant walls. The direct arrivals have been muted before imaging. Most of the targets and walls have ghosts from the unrectified negative parts of the signals. The noise shows up as uncertainty in the direction to the targets but not in the ranges. The data were corrected for different sensitivities of the sensor components before imaging.

The ghosts and some of the noise present in Figure 9 can be reduced by rectifying the data using the hydrophone data as described by equations 9–12 and illustrated in Figures 7 and 8. Figure 10 illustrates the imaging in the same horizontal slices as in Figure 9. The ghosts and the noise are much weaker, and the targets and walls are positioned correctly.

DISCUSSION

This article demonstrates a method for acoustically imaging a very simple environment. A real marine environment is far more complex, with many surfaces and objects that pose challenges to the processing of vector acoustic data. There will need to be a great deal of theoretical development in vector data processing and imaging before this method can be applied to realistic environments. The primary challenges are the multiple overlapping reflections and the unknown sound velocity structure. Vector wavefield decomposition methods can separate and isolate the individual reflections (e.g., Muijs et al., 2004; Paulus and Mars, 2006) that can then be imaged. Alternatively, existing migration concepts can be extended to vector data (e.g., Lüth et al., 2005). It also may be possible to determine velocities using backscattered energy (Wood et al., 1997) that could allow for surveys with fewer receiver locations and smaller spatial apertures.

The direct imaging method shown in this article does not use any phase information between source positions, and the images do not have some of the common artifacts because of frequency and spatial limitations of the data. The primary flaws in these vector-derived images are the directional noise caused by overlapping signals and the limited illumination of the flat surfaces. Incorporating vector data into existing or future imaging methods may reduce artifacts significantly, particularly when the spatial coverage is limited.

The illumination of surfaces and extended structures for vector-based surveys is an unexplored issue. Low-frequency seismic surveys over sedimentary basins produce primarily specular reflections and may require more extensive source and receiver coverage. Some

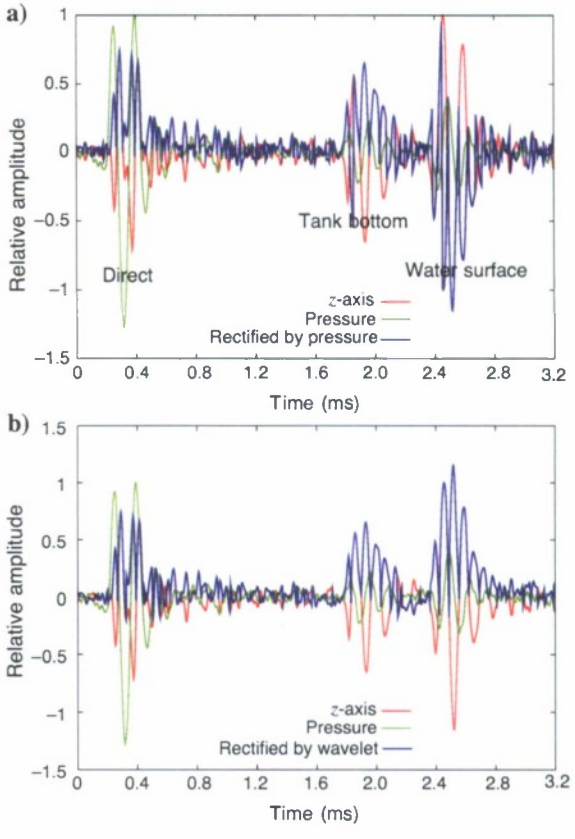

Figure 8. Time series plots of the z-axis accelerometer, the pressure hydrophone, and the rectified z-axis signal. (a) Plot uses the matched hydrophone data as the rectifying series. (b) Plot uses the wavelet correlated with the z-axis data as the rectifying series. The (a) pressure-rectified data, although not perfectly phase matched, show most of the tank bottom and water surface reflections coming from opposite directions. The (b) wavelet-rectified data erroneously place the water surface reflection because of the π-radians phase shift of the free surface reflection.

higher-frequency surveys for near-seafloor structures and objects use primarily diffuse (backscatter) reflections and point diffractions and may require only a few widely spaced survey lines.

Figure 11 compares the vector-imaged volume with a 2D-migrated image generated from the hydrophone data shown in Figure 2.

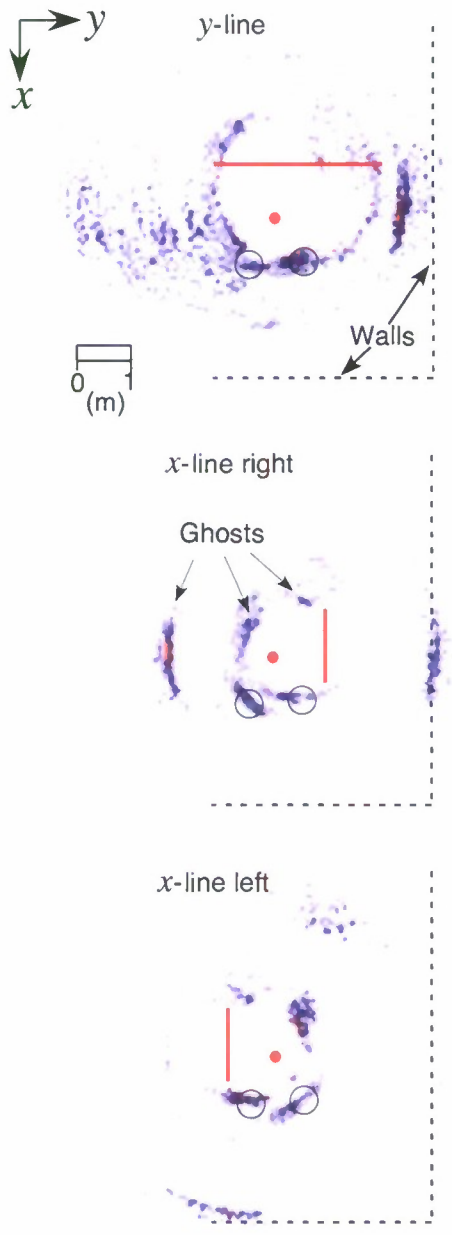

Figure 9. Horizontal slices of 3D volume images of the water tank using unrectified data from three different source lines. The source (red lines), sensor (red dots in center), and targets (black circles) are all at the same depth in these slices in the x-y plane. All of the reflecting and scattering structures have strong ghosts because the data are unrectified. The images were calculated by mapping each time sample to a gridded position using equation 4 and adding the absolute value of the amplitude of that time sample to the corresponding grid. The direct arrivals are not included in these images.

The vector image correctly positions the scattering points and reflecting surfaces in 3D space, whereas 2D migration cannot correctly position scattering points that are outside the horizontal plane of the source line and receiver. This is not a fair test for 2D migration because the survey configuration and the environment in this experiment are not restricted to the vertical plane that 2D migration was designed for. Also, 2D migration is restricted to one direction from the source or receiver line, usually below, whereas the tank environment used here had features in all directions.

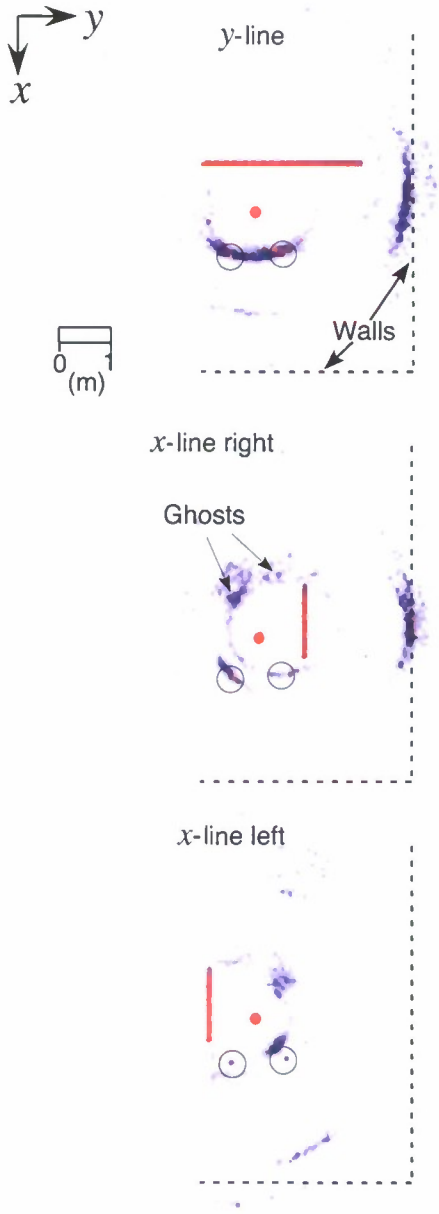

Figure 10. Rectified (pressure-derived) horizontal slices of the volume image of the tank environment. The source (red lines), sensor (red dots in center), and targets (black circles) are all at the same depth in these slices in the x-y plane. The images were formed in the same manner as in Figure 9. Although the rectification is imperfect, most of the ghosts have been eliminated, and the noise has been reduced substantially.

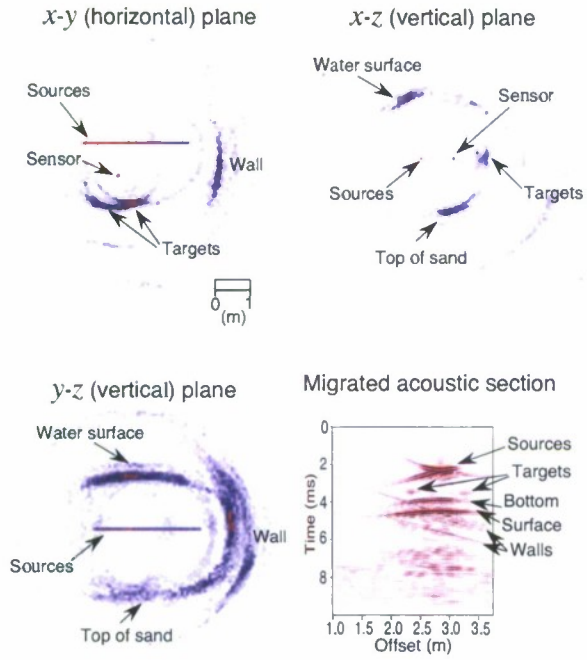

Figure 11. Comparison of three slices of the volume-imaged vector data with a migrated section of the pressure data. These are all imaged using data from the single line of sources shown in Figure 2 and is also the y-line in Figures 9 and 10. The receiver and targets are outside of the slice in the y-z plane. The vector-derived images correctly locate all of the major features, whether they are up or down or in the x- or y-direction. The migrated section places all features in a single half-plane, with the tank bottom, water surface, walls, and targets in the same direction.

A line of vector acoustic data has an advantage over a similar line of scalar hydrophone data in a 3D environment in that the vector data can resolve directional ambiguities and make 3D imaging possible. Existing vector acoustic technology is ready for use in its initial marine surveys and awaits the theoretical developments necessary for imaging more complex environments.

CONCLUSION

This work demonstrates the ability to locate objects and surfaces acoustically in three dimensions using a very limited number of vector acoustic data points. The directional ambiguity inherent to particle motion sensors is removed by rectifying the signals using collocated hydrophone data. Vector data from single shots show that the wave-motion direction can be determined readily for both direct waves and scattered waves when there are few overlapping signals. By measuring the direction and traveltimes of scattered and reflected waves at relatively few locations, it is possible to image the acoustic features of a 3D volume.

The technique presented here is limited to simple environments with a small number of surfaces and targets. With the development of methods for separating the overlapping vector signals and inverting the decomposed wavefield, it may be possible to image geologically realistic 3D environments with significantly reduced source and receiver coverage. A 3D seismic survey may be possible with vector sensors using logistics similar to 2D surveys that use conventional hydrophones.

ACKNOWLEDGMENTS

I wish to thank Roger Richards of the NAVSEA division of the Naval Underwater Warfare Center who loaned the TV-001 sensor and provided technical expertise. I also thank Harry Simpson and Roger Volk of NRL for doing most of the work regarding the tank configuration and setting up the data acquisition. I appreciate the suggestions from the anonymous reviewers who contributed a significant amount to the clarity of this paper plus found several errors in the original manuscript. This work was funded by the Office of Naval Research program element 61153N.

REFERENCES

Berliner, M. J., and J. F. Lindberg, 1996, Acoustic particle velocity sensors: Design, performance, and applications: American Institute of Physics, Conference Proceedings vol. 368, 288853.

Chapman, C. H., 2004, Fundamentals of seismic wave propagation: Cambridge University Press.

Crocker, M. J., and J. P. Arenas, 2003, Fundamentals of the direct measurement of sound intensity and practical applications: Acoustical Physics, **49**, 163–175.

D'Spain, G. L., W. S. Hodgkiss, and G. L. Edmonds, 1991, The simultaneous measurement of infrasonic acoustic particle velocity and acoustic pressure in the ocean by freely drifting swallow floats: IEEE Journal of Ocean Engineering, **16**, 195–207.

Fahy, F. J., 1977, Measurement of acoustic intensity using the cross-spectral density of two microphone signals: Journal of the Acoustical Society of America, **62**, 1057–1059.

———, 1989, Sound intensity: Elsevier Science Publ. Co., Inc.

Kinsler, L. E., A. R. Frey, A. B. Coppens, and J. V. Sanders, 1982, Fundamentals of acoustics: John Wiley & Sons, Inc.

Lindwall, D., 2006, Imaging marine geophysical environments with vector acoustics: Journal of the Acoustical Society of America, **120**, EL43–EL48.

Lüth, S., S. Buske, R. Giese, and A. Goertz, 2005, Fresnel volume migration of multicomponent data: Geophysics, **70**, no. 4, S121–S129.

Muijs, R., J. O. A. Robertsson, and K. Holliger, 2004, Data-driven adaptive decomposition of multicomponent seabed recordings: Geophysics, **69**, 1329–1337.

Paulus, C., and J. I. Mars, 2006, New multicomponent filters for geophysical data processing: IEEE Transactions on Geosciences and Remote Sensing, **44**, 2260–2270.

Pierce, A. D., 1981, Acoustics, An introduction to its physical principles and applications: McGraw-Hill Book Co.

Shipps, J. C., and K. Deng, 2003, A miniature vector sensor for line array applications: OCEANS 2003 Proceedings, 5, 2367–2370.

Wood, W. T., J. F. Gettrust, M. K. Sen, and J. G. Kosalas, 1997, Bottom/subbottom surveying using a new parametric, sidescan sonar: NATO SACLANT Conference on High Frequency Acoustics in Shallow Water.